Earthquakes and Structures, *Vol. 18, No. 4* (*2020*) *467-480*
DOI: https://doi.org/10.12989/eas.2020.18.4.467

Shock absorption of concrete liquid storage tank with different kinds of isolation measures

Wei Jing*[1,2], Peng Chen[1,2a] and Yu Song[1b]

[1]*Key Laboratory of Disaster Prevention and Mitigation in Civil Engineering of Gansu Province, Lanzhou University of Technology, Lanzhou, 730050, PR China*
[2]*Western Engineering Research Center of Disaster Mitigation in Civil Engineering of Ministry of Education, Lanzhou University of Technology, Lanzhou, 730050, PR China*

(*Received November 7, 2019, Revised March 19, 2020, Accepted March 20, 2020*)

Abstract. Concrete rectangular liquid storage tanks are widely used, but there are many cases of damage in previous earthquakes. Nonlinear fluid-structure interaction (FSI) is considered, Mooney-Rivlin material is used for rubber bearing, nonlinear contact is used for sliding bearing, numerical calculation models of no-isolation, rubber isolation, sliding isolation and hybrid isolation concrete rectangular liquid storage tanks are established; dynamic responses of different structures are compared to verify the effectiveness of isolation methods; and influences of earthquake amplitude, bidirectional earthquake and far-field long-period earthquake on dynamic responses are investigated. Results show that for liquid sloshing wave height, rubber isolation cause amplification effect, while sliding isolation and hybrid isolation have reduction effect; displacement of rubber isolation structure is much larger than that of sliding isolation with limiting-devices and hybrid isolation structure; when PGA is larger, wall cracking probability of no-isolation structure becomes larger, and probability of liquid sloshing wave height and structure displacement of rubber isolation structure exceeds the limit is also larger; under bidirectional earthquake, occurrence probabilities that liquid sloshing wave height and structure displacement of rubber isolation structure exceed the limit will be increased; besides, far-field long-period earthquake mainly influences structure displacement and liquid sloshing wave height. On the whole, control effect of sliding isolation is the best, followed by hybrid isolation, and rubber isolation is the worst.

Keywords: concrete; rectangular liquid storage tank; isolation; shock absorption; fluid-structure interaction

1. Introduction

Concrete rectangular liquid storage tanks have been widely used due to its unique advantages, but the aseismic capacity of no-isolation concrete liquid storage tank is often insufficient, as a result, which will be easily damaged by earthquake, and some destruction cases of concrete liquid storage tanks caused by earthquake are shown in Fig. 1 (Sezen *et al*. 2008, Gao *et al*. 2012).

Many researchers have done a lot of works on isolation liquid storage tanks, but most of which are aimed at steel tanks. For rubber isolation, Malhotra (1997) founded that the reduction effect on liquid sloshing wave height was not significant, but overturning moment and hydrodynamic pressure could be significantly reduced. Shrimali and Jangid (2004) studied dynamic responses of liquid storage tanks with different sizes, isolation stiffnesses and dampings using modal superposition method and response spectrum method, respectively. Li *et al*. (2010) found that isolation frequency was the main parameter influencing shock absorption performance of isolation tank. Saha *et al*. (2013) conduct random analysis for rubber isolation liquid storage tank, and found that uncertainty of isolation damping had a great influence on structure peak responses. Sun *et al*. (2016) established a simplified mechanical model of isolation tank considering swinging effect, and obtained that rubber isolation could effectively reduce base shear force, but its reduction effect on liquid sloshing wave height was not significant. Safari and Tarinejad (2016) conducted a parametric study for stochastic dynamic responses of liquid storage tank under near and far field earthquake actions. Shekari *et al*. (2019) used boundary element technique and finite element method to analyze influence of base-isolator system on seismic performance of a 3-D rectangular liquid storage container, and found that the sensitivity of base forces, the maximum hydrodynamic pressure and liquid oscillation were related to base-isolator stiffness.

For liquid storage tank with sliding isolation bearings, Panchal and Jangid (2011) studied dynamic responses of variable frequency pendulum and friction pendulum isolation liquid storage tanks by comparison analysis, and discussed influences of friction coefficient, frequency change factor and structure size on dynamic responses. Zhang *et al*. (2011) proposed a simplified model for compound pendulum isolation liquid storage tank, and proved that isolation was suitable for liquid storage tank with different liquid filling ratios. Moeindarbari *et al*.

*Corresponding author, Ph. D.
E-mail: jingwei3276@163.com
[a]Master Student
E-mail: 260500747@qq.com
[b]Professor
E-mail: 591546531@qq.com

ISSN: 2092-7614 (Print), 2092-7622 (Online)

(a) Wall cracking

(b) Roof collapse

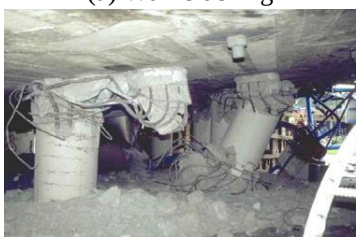

(c) Support system destruction

(d) Overturning failure

Fig. 1 Seismic damages of concrete liquid storage tank

(2014) investigated multiple level performance of seismically isolated elevated storage tank isolated with multi-phase friction pendulum bearing. Bagheri and Farajian (2016) studied the influence of earthquake characteristics on dynamic responses of FPS isolation liquid storage tank. Hashemi and Aghashiri (2017) used an equivalent mechanical model for liquid storage tank with friction pendulum system. Colombo and Almazán (2017) proposed a non-linear isolation system for liquid storage tank, and obtained that effect of the isolation system reduced the limit state probability in the order of 90%. Uckan *et al*. (2018) investigated liquid storage tank with concave sliding bearings subjected to real and simulated near-fault earthquakes. Compagnoni *et al*. (2018) carried out shaking table tests of steel tanks with sliding concave bearings, and found that sliding concave bearings could not significantly control sloshing displacement. Tsipianitis and Tsompanakis (2019) investigated effect of damping modeling on dynamic responses of liquid storage tanks isolated by friction pendulum bearings. Rawat *et al*. (2019) carried out a numerical study of liquid storage tank with friction pendulum system by finite element method, and obtained that base shear force was reduced with the increase of time period of the isolator.

Although many researchers have done extensive researches on isolation liquid storage tank, most of which are on circular steel liquid storage tanks. According to post disaster statistics, destruction types of concrete liquid storage tanks mainly include wall cracking and liquid leakage, in view of the importance and failure characteristics of rectangular liquid storage tank, it is urgent to conduct corresponding seismic response reduction research. At present, Cheng *et al*. (2017), Jing and Cheng (2019) have carried out research on the seismic performance of sliding isolation concrete rectangular liquid storage tank. Besides, although hybrid isolation is an important measure to reduce structure dynamic responses (Cancellara and Angelis 2016), there is lack of reference on hybrid isolation concrete liquid storage tank. In this paper, the liquid was simulated based on subsonic potential flow theory, and fine 3-D numerical calculation models of no-isolation, rubber isolation, sliding isolation with limiting-devices and hybrid isolation concrete rectangular liquid storage tank were established considering nonlinear FSI. The reduction effects of different isolation methods on concrete rectangular liquid storage tank are compared, and the influences of PGA, bidirectional earthquake and far-field long-period earthquake on dynamic responses of rectangular liquid storage tank are investigated.

2. Solution of nonlinear FSI

2.1 Dynamic equation

Assuming that liquid boundary surface S adjacent to structure is S_1, and force $\mathbf{F}_U$ acting on structure boundary caused by liquid pressure can be expressed as

$$-\delta\mathbf{F}_U = -\int_{S_1} p\mathbf{n}\cdot\delta\mathbf{u}dS_1 \tag{1}$$

where $\mathbf{n}$ is normal vector of adjacent interface; p is liquid pressure.

Because of nonlinearity, exact solution of each step needs multiple equilibrium iterations, and nonlinear fluid-structure interaction equation based on subsonic potential flow theory can be obtained (Sussman and Sundqvist, 2003)

$$\begin{bmatrix}\mathbf{0} & \mathbf{0}\\ \mathbf{0} & -\mathbf{M}_{FF}\end{bmatrix}\begin{bmatrix}\Delta\ddot{\mathbf{u}}\\ \Delta\ddot{\phi}\end{bmatrix}+\begin{bmatrix}\mathbf{C}_{UU} & \mathbf{C}_{UF}\\ \mathbf{C}_{FU} & -\left(\mathbf{C}_{FF}+\left(\mathbf{C}_{FF}\right)_S\right)\end{bmatrix}\begin{bmatrix}\Delta\dot{\mathbf{u}}\\ \Delta\dot{\phi}\end{bmatrix}+\begin{bmatrix}\mathbf{K}_{UU} & \mathbf{K}_{UF}\\ \mathbf{K}_{FU} & -\left(\mathbf{K}_{FF}+\left(\mathbf{K}_{FF}\right)_S\right)\end{bmatrix}\begin{bmatrix}\Delta\mathbf{u}\\ \Delta\phi\end{bmatrix}=\begin{bmatrix}\mathbf{0}\\ \mathbf{0}\end{bmatrix}-\begin{bmatrix}\mathbf{F}_U\\ \mathbf{F}_F+\left(\mathbf{F}_F\right)_S\end{bmatrix} \tag{2}$$

where $\mathbf{M}_{FF}$ is liquid mass matrix; $\mathbf{M}_{SS}$, $\mathbf{C}_{SS}$ and $\mathbf{K}_{SS}$ are mass, damping and stiffness matrices of structure, respectively; $\mathbf{C}_{UU}$, $\mathbf{C}_{FU}$, $\mathbf{C}_{UF}$ and $\mathbf{C}_{FF}$ are damping matrices of the structure itself, the liquid caused by the structure, the structure caused by the liquid and the liquid itself, respectively; and $\mathbf{K}_{UU}$, $\mathbf{K}_{FU}$, $\mathbf{K}_{UF}$ and $\mathbf{K}_{FF}$ are the stiffness matrices of the structure itself, the liquid caused by the structure, the structure caused by the liquid and the liquid itself, respectively; $\mathbf{F}_{SS}$ is the load vector acting on structure; $\mathbf{F}_U$, $\mathbf{F}_F$ and $(\mathbf{F}_F)_S$ are the forces acting on structure boundary caused by liquid pressure, volume force and area force, respectively.

$\mathbf{F}_F$ and $(\mathbf{F}_F)_S$ can be obtained by volume and surface integrations (Sussman and Sundqvist 2003)

$$\mathbf{F}_F = \int_V \left(\frac{\partial \rho}{\partial h} \dot{h} \delta\phi - \rho \nabla \phi \right) dV \tag{3}$$

$$\left(\mathbf{F}_F\right)_S = \int_S -\rho \dot{\mathbf{u}} \cdot \mathbf{n} \delta\phi dS \tag{4}$$

where V is liquid domain; S is boundary of liquid domain; $\mathbf{n}$ is vector in the internal normal direction of S; and $\dot{\mathbf{u}}$ is movement velocity vector of S.

2.2 Boundary conditions

There exist three kinds of boundary conditions for liquid storage tank under earthquake (Chen *et al*., 2007), namely, wall boundary Γ_w, bottom boundary Γ_b and liquid free surface boundary Γ_f. On the free surface Γ_f, dynamic and kinematic boundary conditions should be satisfied.

Assuming that $\mathbf{L}(\xi, \gamma, \eta)$ is position vector of a particle on the liquid free surface, then the kinematic boundary condition on the liquid free surface Γ_f is

$$\frac{\mathrm{D}\mathbf{L}}{\mathrm{D}t} = \left(\frac{\partial}{\partial t} + U \cdot \nabla \right) \mathbf{L} = \mathbf{U}, \quad \Gamma_f \tag{5}$$

where D/Dt is derivatives to the time described by Lagrange; and $\mathbf{U}$ is velocity vector. Assuming that atmospheric pressure is 0, and the dynamic boundary condition on the liquid free surface Γ_f can be obtained by Bernoulli equation

$$\frac{\mathrm{D}\phi}{\mathrm{D}t} = -g\eta + \frac{1}{2}\left|\nabla\phi\right|^2, \quad \Gamma_f \tag{6}$$

where g is gravity acceleration; η is free surface sloshing height. Boundary conditions corresponding to wall Γ_w and bottom Γ_b is

$$\frac{\partial \phi}{\partial n} = V_n\left(x, y, z\right), \quad \Gamma_w \text{ and } \Gamma_b \tag{7}$$

where $V_n(x,y,z)$ is outer normal velocity; $\partial / \partial n$ is external normal derivative.

On the fluid-structure interaction interface, the following conditions should be satisfied

$$\begin{cases} \mathbf{u}_s = \mathbf{u}_f, & \left(\text{Displacement condition}\right) \\ \sigma_s \cdot \mathbf{n}_s = \sigma_f \cdot \mathbf{n}_f, & \left(\text{Stress condition}\right) \end{cases} \tag{8}$$

where $\mathbf{u}_f$ and $\mathbf{u}_s$ are the displacement vectors of liquid and structure on the FSI interface; $\mathbf{n}_f$ and $\mathbf{n}_s$ are the outer normal vectors on the FSI interface; σ_f and σ_s are the stresses of liquid and structure on the FSI interface

3. Engineering application research

3.1 Geometric parameters

The geometric parameters of the concrete rectangular liquid storage tank are shown in Fig. 2.

3.2 Isolation scheme

At the structure bottom, 8 isolation bearings are arranged in total, scheme I is rubber isolation, as shown in Fig. 3(a); scheme II is sliding isolation, as shown in Fig. 3(b); scheme III is hybrid isolation, as shown in Fig. 3(c).

3.2.1 Rubber isolation

To avoid structure resonance, isolation period should be far away from the predominant period of earthquake wave, and isolation period T_{iso} can be calculated by Eqs. (9) - (11).

$$T_{iso} = 2\pi \sqrt{\frac{M_i + M_s}{K_{iso}}} \tag{9}$$

$$K_{iso} = nk_{iso} \tag{10}$$

$$M_i = \frac{\tanh\left[0.866\left(L / h_w\right)\right]}{0.866\left(L / h_w\right)} M_L \tag{11}$$

where K_{iso} is stiffness of isolation layer; M_i is the liquid mass moving along with the structure (ACI Committee 350, 2006); M_s is structure mass; k_{iso} is equivalent stiffness of a rubber isolation bearing; n is number of isolation bearings; L is structure length parallel to the main direction of earthquake action; h_w is liquid level height; M_L is total mass of liquid.

3.2.2 Sliding isolation

In order to solve the problems of large and residual displacements of sliding isolation liquid storage tank, displacement limiting-devices are arranged in four corners of the tank (Cheng *et al*. 2018), and the details are shown in Fig. 4.

The maximum horizontal displacement of sliding isolation liquid storage tank should satisfy the following requirements, namely

(1) Safety use (Cheng *et al*. 2017)

$$\Delta S_1 \le 150 \text{ mm} \tag{12}$$

(2) Deformation capacity of limiting-device

As shown in Fig. 5, the displacement limit of isolation layer is depended on the principle of deformation coordination of displacement limiting-device.

Where ΔS_2 is the displacement limit depending on

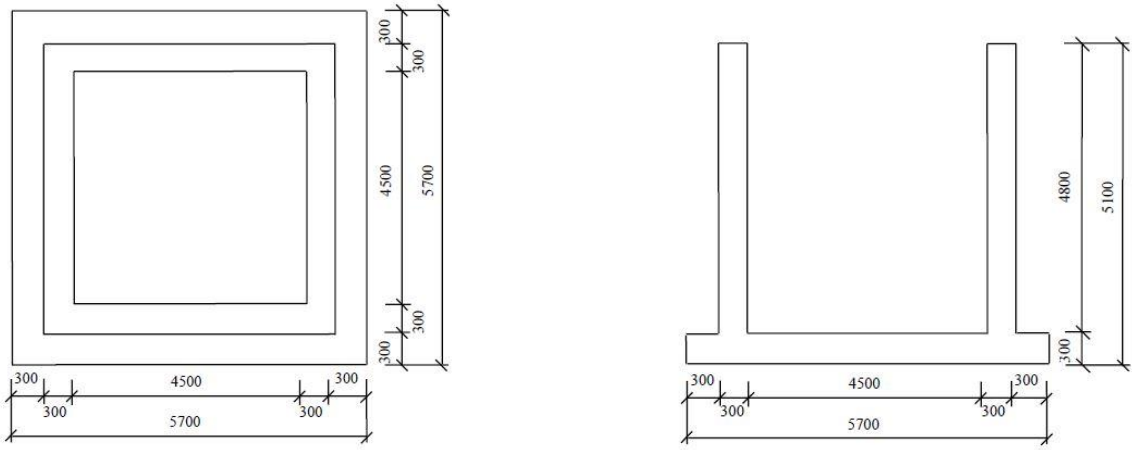

(a) Plan (b) Elevation

Fig. 2 Geometric model (unit: mm)

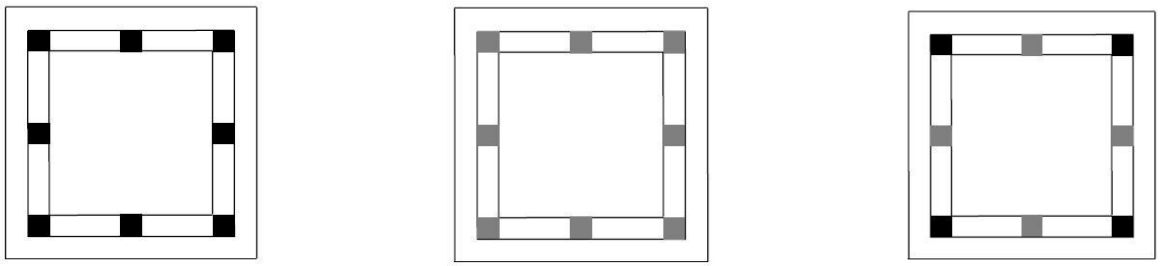

(a) Rubber isolation (b) Sliding isolation (c) Hybrid isolation

Fig. 3 Isolation scheme

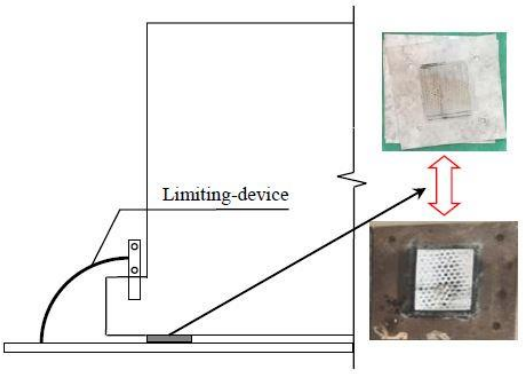

Fig. 4 Sketch of sliding isolation structure with limiting-devices

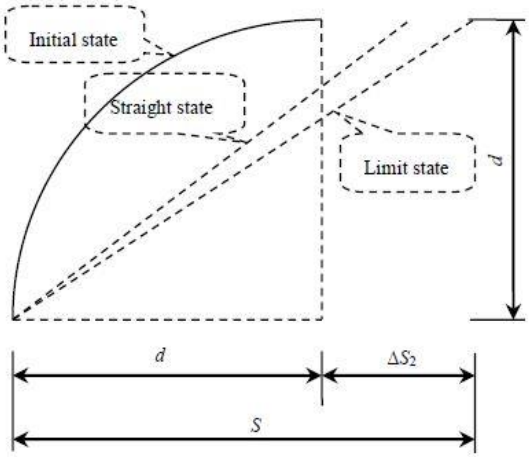

Fig. 5 Deformation of limiting-device

deformation capacity of limiting-device, S is the level projection length when the device reaches the limit state, d is the radius of the arc limiting-device, and ε_u is the ultimate tensile strain of the limiting-device material.

Therefore, the displacement limit of isolation layer should be a smaller value between ΔS_1 and ΔS_2.

3.2.3 Hybrid isolation

Initial horizontal stiffness K_0 of the isolation layer can be superposition of the horizontal stiffness of the rubber isolation bearings K'_{iso} and the initial horizontal stiffness K_s of the friction isolation bearings, and the yield shear force F_{Q_0} of the hybrid isolation layer is

$$F_{Q_0}=F_{Q_{sy}}+K'_{iso}X_y=F_{Q_{sy}}+mk_{iso}X_y \tag{14}$$

where $F_{Q_{sy}}$ is yield shear force of friction sliding bearings; K'_{iso} is horizontal stiffness provided by rubber bearings; X_y is yield displacement of friction sliding bearing; m is number of rubber bearings.

Because the yield displacement X_y of the friction

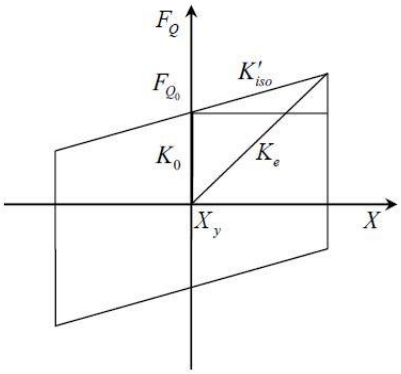

Fig. 6 Restoring force curve of hybrid isolation layer

Table 1 Mooney-Rivlin material model parameters of rubber (unit: N/mm^2)

Parameters	C1	C2	C3	C4	C5	C6
Values	206000	1858	4100	100	0	28.1

Table 2 Material parameters of the limiting-device

Elastic modulus E/Pa	Poisson's ratio ν	Yield strength σ/MPa	Density ρ/kg/m^3	Strain hardening modulus E/Pa	Yield strain ε	Maximum plastic strain ε_u
2×10^{11}	0.3	235	7800	2×10^9	0.001	0.02

sliding bearing is very small, therefore, the approximate shear yield of the isolation layer can be obtained by Eq. (15)

$$F_{Q_0} \approx F_{Q_{sy}} = \mu\lambda Mg \tag{15}$$

where μ is friction coefficient of sliding isolation bearing; λ is the proportion of superstructure weight borne by friction sliding bearings; M is total mass of superstructure; g is gravity acceleration.

The period of hybrid isolation can be calculated by Eq. (16)

$$T_e = 2\pi\sqrt{\frac{M_i + M_s}{K_e}} = 2\pi\sqrt{\frac{M_i + M_s}{K'_{iso}X + F_{Q_0}}X} = 2\pi\sqrt{\frac{M_i + M_s}{mk_{iso}X + \mu\lambda Mg}X} \tag{16}$$

The model of restoring force of hybrid isolation layer is shown in Fig. 6.

4. Numerical example

4.1 Calculation model

Assuming that concrete material is linear elastic, its modulus of elasticity is 3×10^{10} Pa, Poisson's ratio is 0.20, density is 2500 kg/m^3, and 3-D Solid element is used to simulate concrete structure, which is 8-nodes and iso-parametric displacement-based finite element; in addition to the displacement-based finite element, special mixed-interpolated element is also available, in which the displacement and pressure are interpolated and the element is suitable for analyses in which 3-D state of stress is required. Assuming that liquid is irrotational, inviscid and incompressible, subsonic potential flow theory is used for liquid material model, the potential-based fluid element can simulate fluid-structure interaction and free surface, respectively. Liquid depth is 3.6 m, its density is 1000 kg/m^3, bulk modulus is 2.3×10^9 Pa, and 3-D Fluid element with 8-nodes is used for the liquid. FSI boundary is set on the FSI interface, and free surface is set on the liquid surface.

Lateral-vertical coupling and predicting instability should be taken into account nonlinear modelling of rubber bearings (Vemuru *et al*. 2014, Mazza *et al*. 2017). Mooney-Rivlin strain energy density function is used to describe the hyperelastic constitutive model of rubber isolation bearings. The model assumes that rubber is incompressible and isotropic before deformation, which can well describe the mechanical properties of rubber materials with deformation less than 150%, and fully meet the needs of performance calculation in practical application of rubber materials. The size of rubber isolation bearing is 0.3 m×0.3 m×0.2 m，the number is 8，density is 850kg/m^3, bulk modulus is 2.72×10^9 Pa, and Poisson's ratio is 0.5. Material parameters of rubber isolation are shown in the Table 1 (Yuan 1993).

Assuming that the strain energy density is a polynomial function of the principal strain invariant, the strain energy function should be symmetrical to three main elongation under isotropic condition, and the strain energy density function W described by the invariant of deformation tensor can be expressed as

$$W = \sum_{i+j-1}^{n} C_{ij}\left(I_i - 3\right)^i \left(I_j - 1\right)^j \tag{17}$$

where C_{ij} is material constants generally determined by experiment; I is deformation tensor invariant, I_i and I_j are the i-th and the j-th Green strain invariants.

Nonlinear modeling of sliding bearings should take into account that friction force and lateral stiffness present continuous variation during an earthquake because they are proportional to the axial load. Moreover, further changes of the friction force result from variation of the friction coefficient depending on the sliding velocity, with reduction at the onset of motion and motion reversals, axial pressure and temperature at the sliding surface (Mosqueda *et al*. 2004, Mazza and Mazza 2016). The size of sliding isolation bearing is 0.3 m×0.3 m×0.2 m, the number is 8. For sliding isolation bearings, the mechanical behavior is simulated by setting 3-D contact, the normal contact w-function parameter is 1×10^{-12}, sticking velocity is 0 m/s, contact surface extension factor is 0.001, and the friction coefficient is assumed to be 0.02. Constraint function is used to solve nonlinear contact. Bilinear material model and Beam element are used to simulate the limiting-device, the material parameters are shown in Table 2 (Cheng *et al*. 2017).

In May 18, 1940, Imperial Valley earthquake occurred, the world's first seismic waveform is recorded in El-Centro station, and North-South direction record is used in this

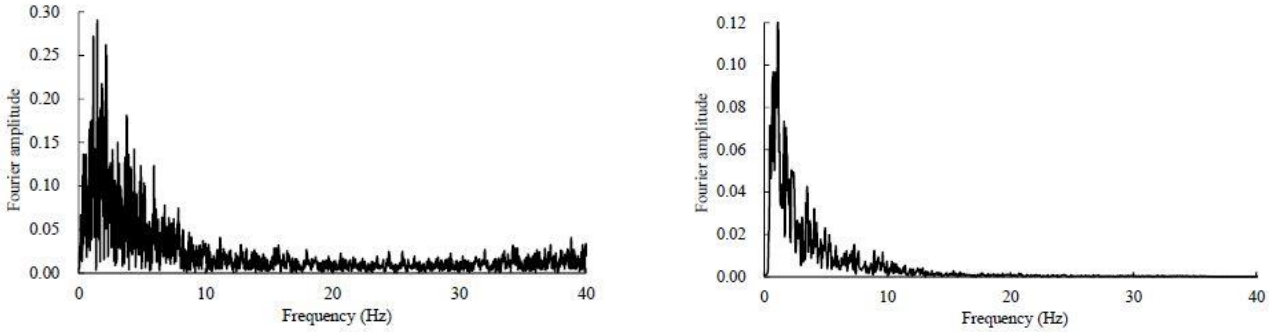

(a) El-Centro wave (b) Tianjin wave

Fig. 7 Fourier spectra

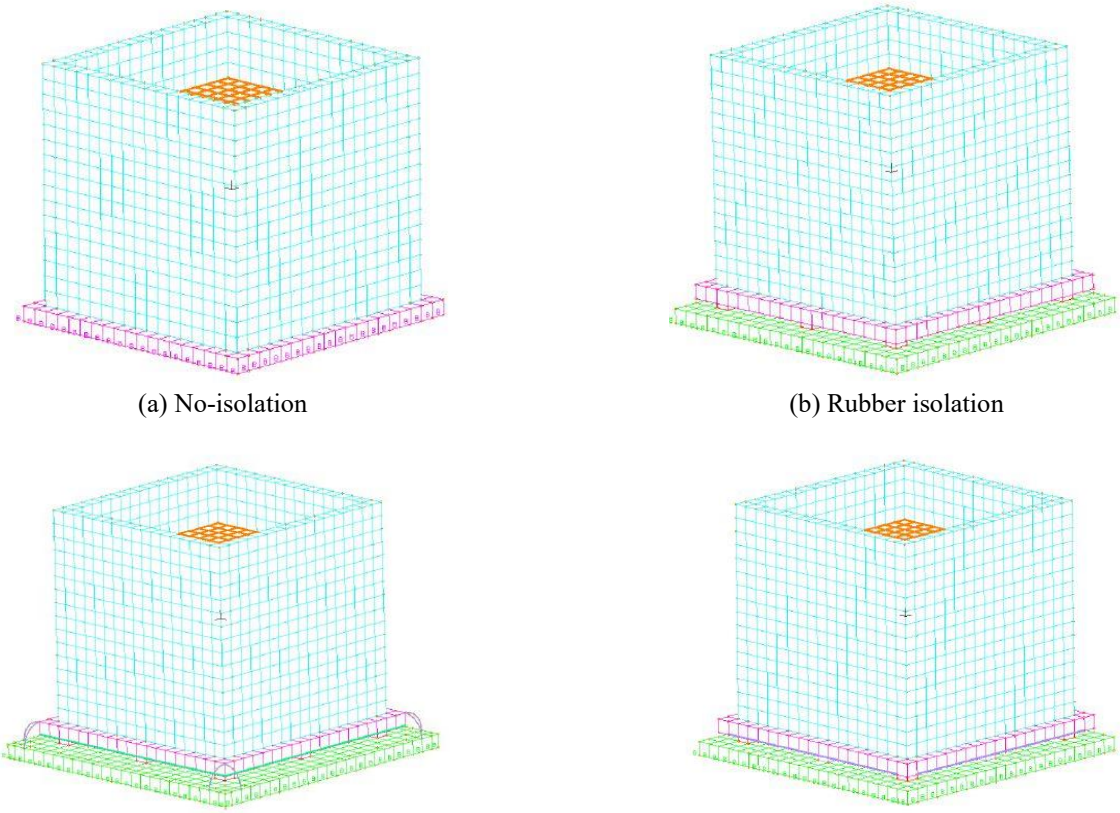

(a) No-isolation (b) Rubber isolation

(c) Sliding isolation (d) Hybrid isolation

Fig. 8 Numerical calculation models

paper. In November 25, 1976, Tianjin earthquake in Ninghe occurred, and North-South direction record in Tianjin hospital station is used in this paper.

El-Centro wave has been widely used in the research of structural dynamic response in the engineering field. Tianjin wave has long period characteristics and has been widely used in the research and analysis of dynamic response of liquid storage tank. In addition, the computational model involves complex fluid structure coupling problems, in order to improve the computational efficiency, El-Centro wave and Tianjin wave are selected.

Fourier spectra corresponding to the two seismic waves are shown in Fig. 7, and the predominant frequencies are 0.56 s and 0.94 s, respectively. The numerical calculation models

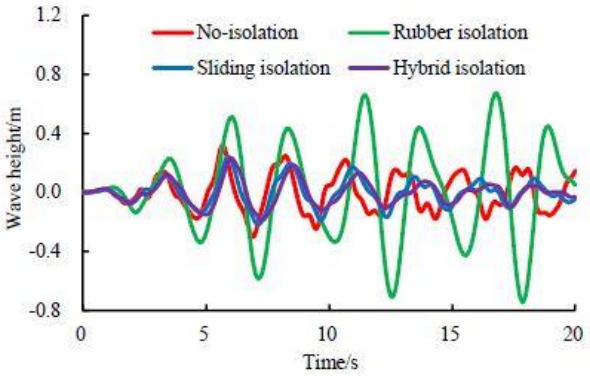

Fig. 9 Liquid sloshing wave height (PGA=0.22 g)

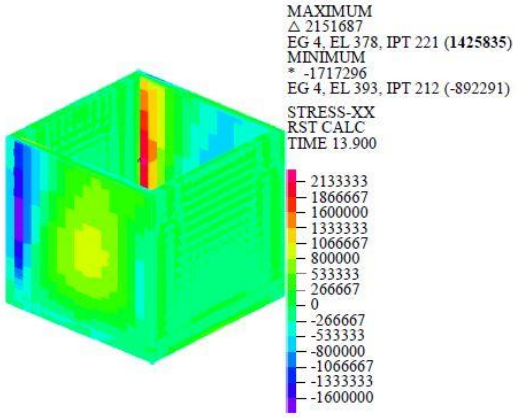

(a) No-isolation

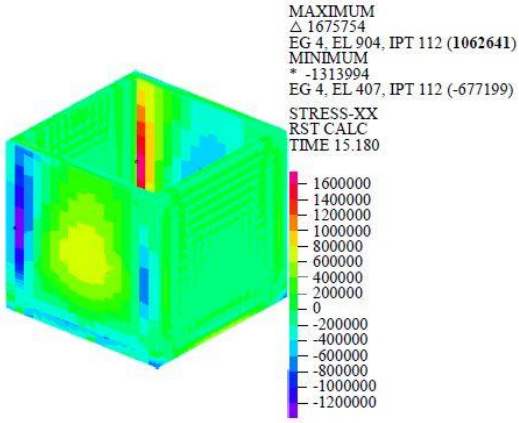

(b) Rubber isolation

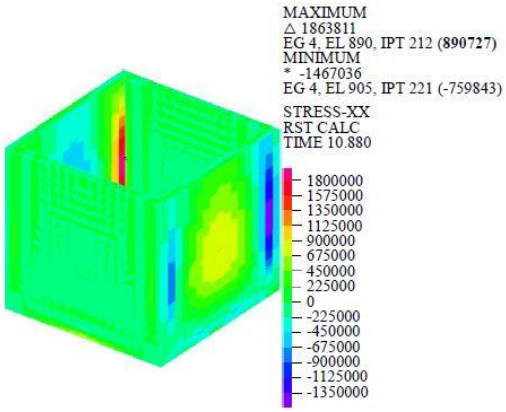

(c) Sliding isolation

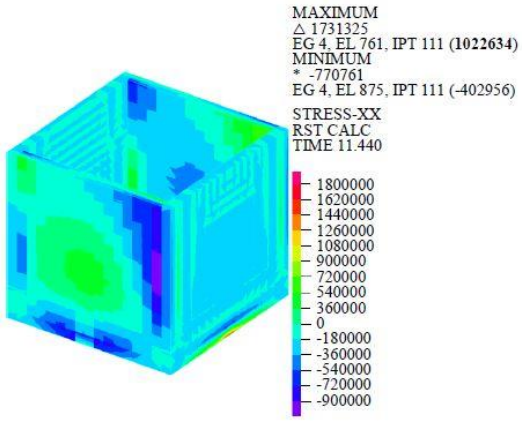

(d) Hybrid isolation

Fig. 10 Wall stress (PGA=0.22 g)

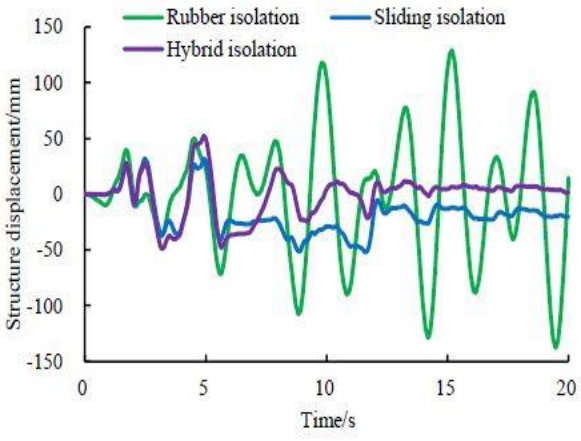

Fig. 11 Structure displacement (PGA=0.22 g)

of concrete rectangular liquid storage tank established by element software ADINA (Automatic Dynamic Incremental Nonlinear Analysis) are shown in Fig. 8. ADINA User Interface can automatically generate fluid-structure interface elements along the boundary between the fluid and structure, so it is not artificially needed to define fluid-structure potential-interfaces. Overall, ADINA has strong advantages in solving complex problems such as structure nonlinearity and fluid-solid interaction.

4.2 Dynamic responses

In view of the two most common failure modes of concrete liquid storage tank are wall cracking and liquid overflow, besides, the possibility of displacement exceeding the limit is larger after taking the isolation measures. Therefore, liquid sloshing wave height, wall stress and structure displacement are chosen as the most important research objects, when PGA is 0.22 g, the three kinds of dynamic responses are shown in Figs. 9 - 11.

(1) Liquid sloshing wave height

As shown in Fig. 9, when PGA is 0.22 g, the maximum liquid sloshing wave heights corresponding to no-isolation, rubber isolation, sliding isolation and hybrid isolation concrete rectangular storage tanks are 0.319 m, 0.744 m, 0.241 m and 0.232 m, respectively. Compared with no-isolation, rubber isolation has amplification effect on the liquid sloshing wave height, and the amplification factor is close to 2. In contrast, sliding isolation and hybrid isolation have good control effect on liquid sloshing wave height.

(2) Wall stress

As shown in Fig. 10, when PGA is 0.22 g, the maximum wall tensile stresses corresponding to no-isolation, rubber isolation, sliding isolation and hybrid isolation concrete rectangular storage tanks are 1.426 MPa, 1.063 MPa, 0.891 MPa and 1.023 MPa, respectively. It can be seen that the

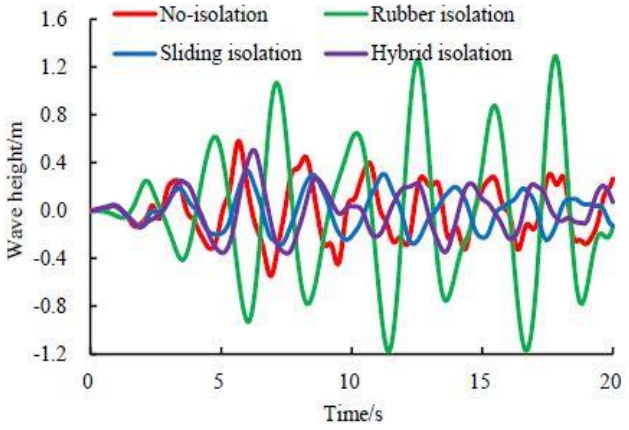

Fig. 12 Liquid sloshing wave height (PGA=0.40 g)

three kinds of isolation method have obvious control effects on the wall tensile stress, which is meaningful for wall crack control.

As shown in Fig. 11, the maximum displacement and residual displacement of rubber isolation structures is much larger than those of sliding isolation structure with limiting-devices and hybrid isolation structure, and it is close to the displacement limit. On the contrary, the maximum displacements of sliding isolation structure with limiting-devices and hybrid isolation structure are far less than the displacement limit, and the final residual displacement is very small. Besides, although the maximum displacement of hybrid isolation structure is larger than that of sliding isolation structure with limiting-devices, the residual displacement of hybrid isolation structure is less than that of sliding isolation structure with limiting-devices. Thus it can be seen that due to the larger displacement and residual displacement, rubber isolation will affect the normal use of liquid storage tank, but sliding isolation structure with limiting-devices and hybrid isolation structure can all be used without any further repair after the end of the earthquake.

4.3 Influence of PGA on dynamic responses

In order to study influences of PGA on dynamic responses, PGA is adjusted to 0.40 g. In this case, calculation results of liquid sloshing wave height, wall stress and structure displacement are shown in Figs. 12 - 14; and influences of PGA on dynamic responses are shown in Table 3.

(1) Liquid sloshing wave height

As shown in Fig. 12, when PGA is 0.40 g, the maximum liquid sloshing wave heights corresponding to no-isolation, rubber isolation, sliding isolation and hybrid isolation concrete rectangular storage tanks are 0.579 m, 1.291 m, 0.334 m and 0.506 m, respectively. Compared with no-isolation, rubber isolation has amplification effect on the liquid sloshing wave height, and the amplification factor is larger than 2. In contrast, sliding isolation has a good control effect on liquid sloshing wave height, but the liquid sloshing wave height of hybrid isolation structure is close to the liquid sloshing wave height of the no-isolation structure.

(2) Wall stress

As shown in Fig. 13, when PGA is 0.40 g, the maximum wall tensile stresses corresponding to no-isolation, rubber isolation, sliding isolation and hybrid isolation concrete rectangular liquid storage tanks are 1.843 MPa, 1.202 MPa, 0.896 MPa and 1.190 MPa, respectively. It can be seen that the wall tensile stress of no-isolation structure is close to the tensile strength of concrete, and the three kinds of isolation method have obvious control effects on the wall tensile stress, which is meaningful for wall crack control under strong earthquake.

(3) Structure displacement

As shown in Fig. 14, when PGA is 0.40 g, structure displacements corresponding to rubber isolation and hybrid isolated structures are large, and displacement of rubber isolation structure may affect the normal use of liquid storage structure; on the contrary, displacement of sliding isolation structure is still small due to limiting-devices.

As shown in Table 3, for the no-isolation structure, there is an approximate linear relationship between liquid sloshing wave height and PGA, after isolation being taken, although liquid sloshing wave height is positively related to PGA, it no longer satisfies the linear relationship, and the control effect of sliding isolation on liquid sloshing wave height is the most notable under two kinds of PGAs. The control effect of isolation on wall tensile stress increases with the increase of PGA, and the control effect of sliding isolation on wall tensile stress is the most significant. The maximum horizontal displacement of rubber isolation structure increases significantly with the increase of PGA, when PGA is 0.40 g, the maximum horizontal displacement may affect the normal use of the structure; when PGAs are 0.22 g and 0.40 g, the maximum horizontal displacements of sliding isolation structure with limiting-devices are small; when PGA is 0.22 g, the maximum horizontal displacement of hybrid isolation structure is small, when PGA increases to 0.40 g, the maximum horizontal displacement may also affect the normal use of the structure.

4.4 Influence of earthquake direction on dynamic responses

In our previous research on dynamic responses of sliding isolation liquid storage tank, it has been found that the more the dimension of seismic action is, the greater the dynamic responses will be (Cheng *et al*. 2019). It is possible to include vertical component of seismic excitations in the procedure, and it can be predicted that the dynamic responses will be increased after considering the vertical component. In order to investigate seismic responses of concrete rectangular liquid storage tank with different isolation systems subjected to bidirectional earthquake, seismic responses of four types of structures (no-isolation structure, rubber isolation, sliding isolation structure, hybrid isolation) are compared. The ratio of PGAs in the two horizontal directions is adjusted to 1:0.85. Calculation results of sloshing wave height, wall stress and structure displacement under bi-directional earthquake are shown in

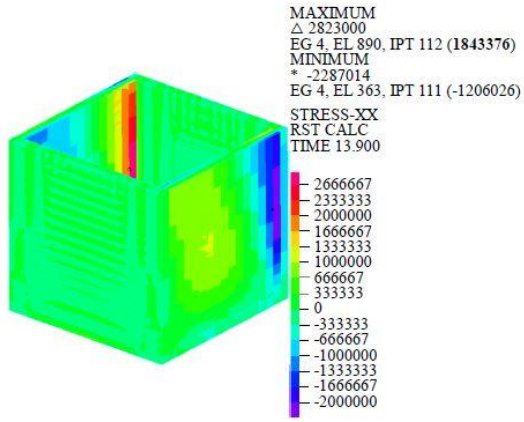

(a) No-isolation

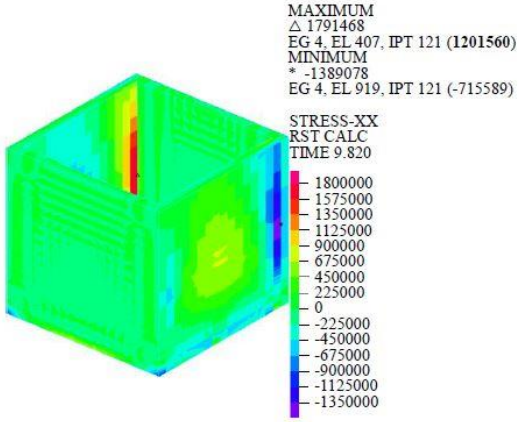

(b) Rubber isolation

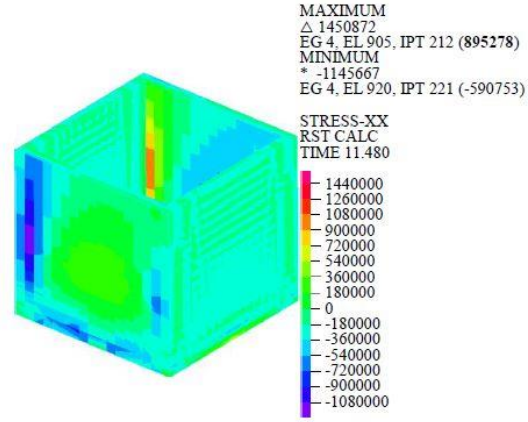

(c) Sliding isolation

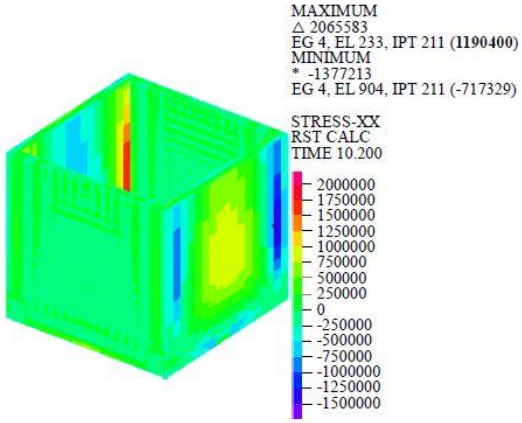

(d) Hybrid isolation

Fig. 13 Wall stress (PGA=0.40 g)

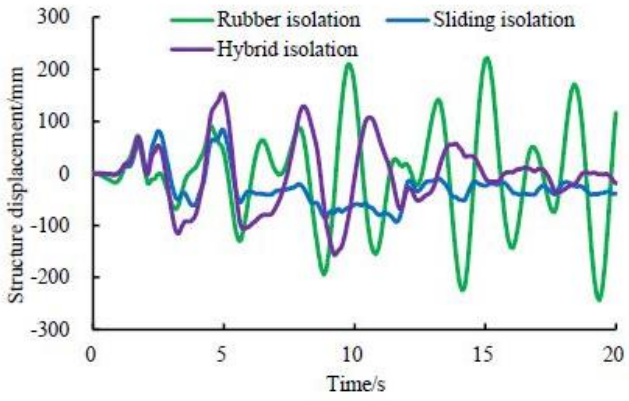

Fig. 14 Structure displacement (PGA=0.40 g)

Table 3 Influence of PGA on dynamic responses

Dynamic responses	PGA	Structure type			
		No-isolation	Rubber isolation	Sliding isolation	Hybrid isolation
Wave height / m	0.22 g	0.319	0.744	0.241	0.232
	0.40 g	0.579	1.291	0.334	0.506
Wall tensile stress / MPa	0.22 g	1.426	1.063	0.891	1.023
	0.40 g	1.843	1.202	0.896	1.190
Structure displacement / mm	0.22 g	——	137.575	50.018	52.253
	0.40 g	——	243.165	93.087	156.747

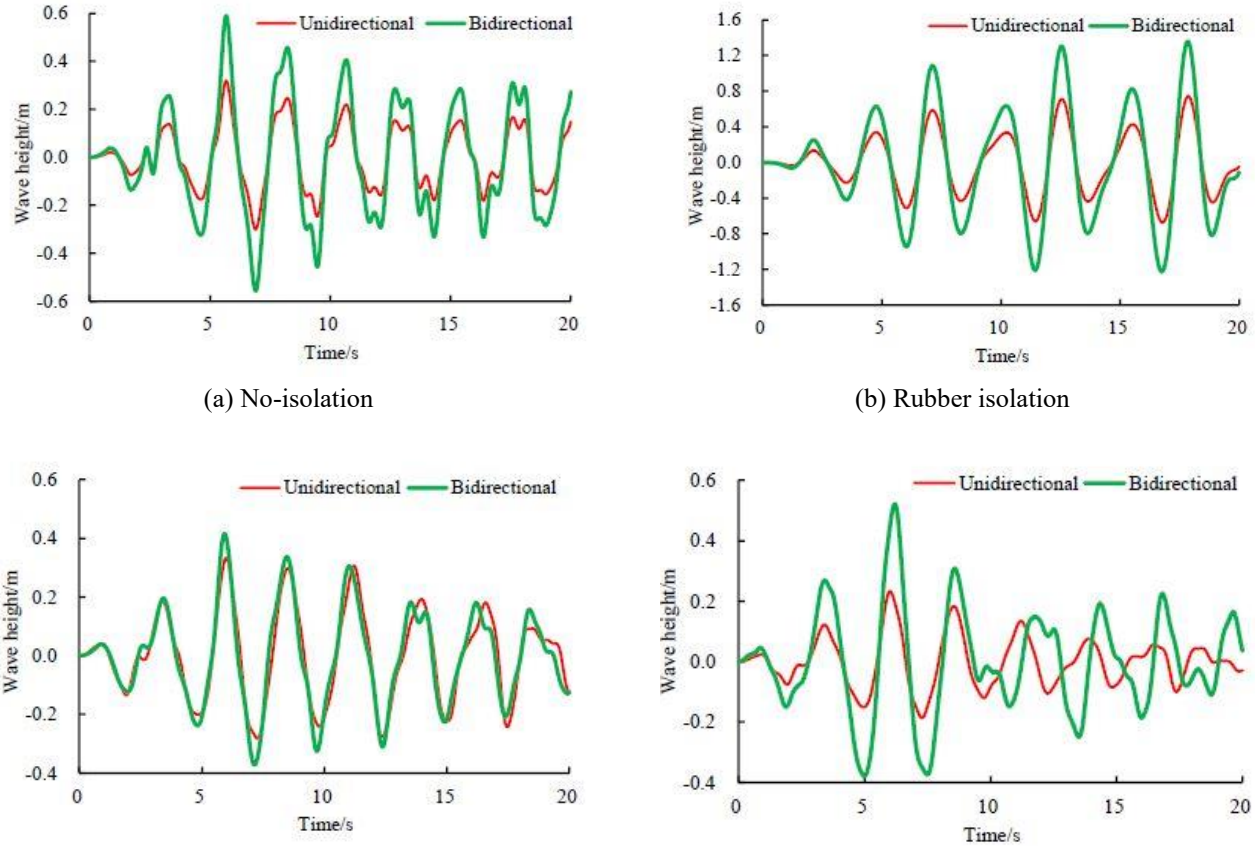

(a) No-isolation (b) Rubber isolation

(c) Sliding isolation (d) Hybrid isolation

Fig. 15 Influence of bi-directional earthquake on liquid sloshing wave height

Figs. 15 - 17, and the maximum values are summarized in Table 4.

(1) Liquid sloshing wave height

As shown in Fig. 15, the maximum wave heights corresponding to no-isolation, rubber isolation, sliding isolation and hybrid isolation are 0.319 m, 0.744 m, 0.241 m and 0.232 m under unidirectional seismic action; after bidirectional earthquake action being considered, these values are increased to 0.589 m, 1.356 m, 0.416 m and 0.517 m. Especially for rubber isolation, liquid sloshing wave height is very large under bidirectional seismic action, which is easy to cause liquid overflow.

(2) Wall stress

As shown in Fig. 16, the maximum wall stresses of no-isolation, rubber isolation, sliding isolation and hybrid isolation are 1.426 MPa, 1.063 MPa, 0.891 MPa and 1.023 MPa under unidirectional seismic action; after bidirectional earthquake action being considered, these values are increased to 1.631 MPa, 1.109 MPa, 0.899 MPa and 1.043 MPa. Wall tensile stress of no-isolation structure is greatly influenced by the bi-directional earthquake, after isolation being taken, influence of bi-directional earthquake actions on wall tensile stress is decreased, and wall tensile stress corresponding to sliding isolation is the minimum under bi-directional seismic actions.

(3) Structure displacement

Table 4 Effect of bidirectional earthquake on the maximum dynamic responses

Dynamic responses	Earthquake direction	Structure type			
		No-isolation	Rubber isolation	Sliding isolation	Hybrid isolation
Wave height /m	Unidirectional	0.319	0.744	0.241	0.232
	Bidirectional	0.589	1.356	0.416	0.517
Wall tensile stress /MPa	Unidirectional	1.426	1.063	0.891	1.023
	Bidirectional	1.631	1.109	0.899	1.043
Structure displacement /mm	Unidirectional	——	137.575	50.018	52.253
	Bidirectional	——	164.900	94.247	70.234

As shown in Fig. 17, the maximum structure displacements corresponding to rubber isolation, sliding isolation and hybrid isolation are 137.575 mm, 50.018 mm and 52.253 mm under unidirectional seismic action; after bidirectional earthquake action being considered, these values are increased to 164.900 mm, 94.247 mm and 70.234 mm. It is shown that bidirectional seismic action will significantly increase the displacement response of isolation structures.

By further summarizing Figs. 14 - 16 and Table 4, it is shown that liquid sloshing wave height, wall tensile stress and structure displacement under bidirectional seismic

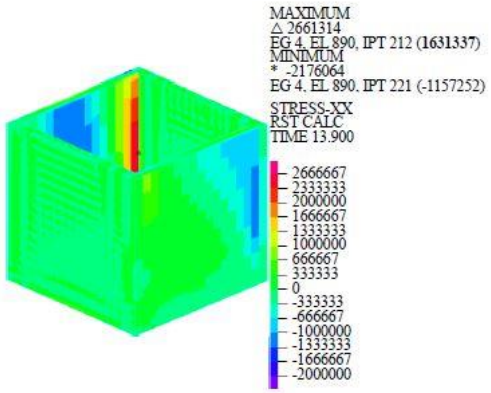

(a) No-isolation

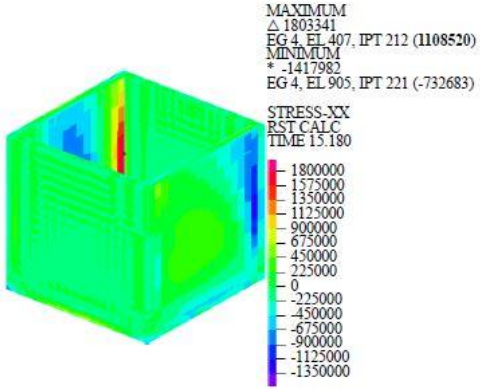

(b) Rubber isolation

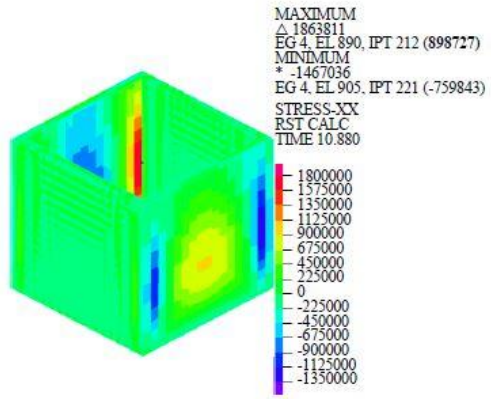

(c) Sliding isolation

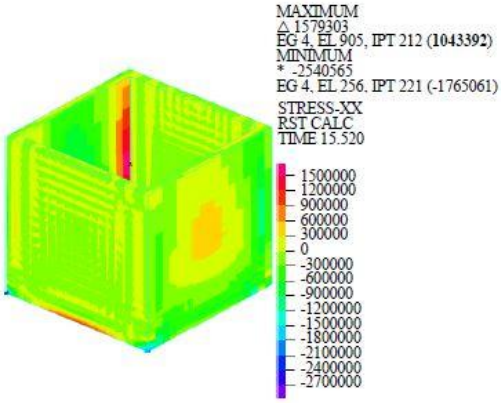

(d) Hybrid isolation

Fig. 16 Influence of bi-directional earthquake on wall stress

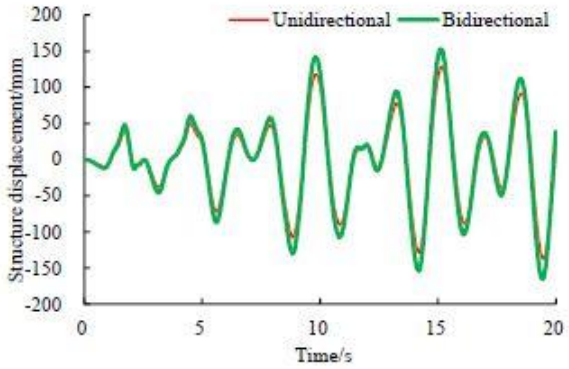

(a) Rubber isolation

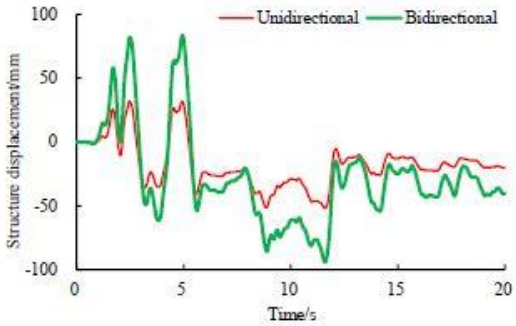

(b) Sliding isolation

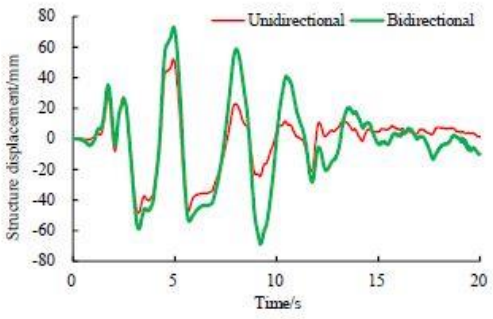

(c) Hybrid isolation

Fig. 17 Influence of bi-directional earthquake on structure displacement

Table 5 Effect of far-field long-period earthquake on the maximum dynamic responses

Dynamic responses	Earthquake wave	Structure type			
		No-isolation	Rubber isolation	Sliding isolation	Hybrid isolation
Wave height / m	El-Centro wave	0.319	0.744	0.241	0.232
	Tianjin wave	0.497	0.814	0.312	0.372
Wall tensile stress / MPa	El-Centro wave	1.426	1.031	1.115	1.123
	Tianjin wave	1.314	1.159	1.131	1.146
Structure displacement / mm	El-Centro wave	——	137.575	50.018	52.253
	Tianjin wave	——	162.316	102.436	138.182

action are larger than that of unidirectional seismic action, and for liquid sloshing wave height, the amplification coefficient is about 2.0; besides, the amplification coefficient corresponding to structure displacement is also large. After isolation being taken, the amplification coefficient for wall tensile stress is relatively small. On the whole, in order to ensure the safety of concrete liquid storage tank, it is necessary to consider bidirectional seismic action

4.5 Effect of far-field long-period earthquake on dynamic responses

The significant feature of liquid storage tank is that sloshing period increases with the increase of structure size, long-period earthquake may cause the resonance response of liquid sloshing, so the damage cases of liquid storage tanks under action of far-field long-period earthquakes are very common. For example, one earthquake occurred in the central Sea of Japan in 1983, which caused liquid leakage of 13 liquid storage tanks in Niigata city, and the distance from the city to the epicenter is about 270 kilometers. Meanwhile, some tank tops were also destroyed due to the impact force of liquid sloshing. In 1993, a large number of tanks located at Niigata Basin occurred significant liquid sloshing during Nanseioki earthquake, and the maximum amplitude of liquid sloshing wave height of those tanks reached 1.7 m. In 2003, Tokachioki earthquake in Japan happened, 7 oil storage tanks were seriously damaged due to violent liquid sloshing under action of far-field long-period earthquake (Zama 2004). Therefore, in order to investigate the reduction effect of isolation measure on the liquid storage tank, it is necessary to study dynamic responses of isolation structure under far-field long-period earthquake. Comparisons of the maximum dynamic responses under near-field El-Centro earthquake and far-field long-period Tianjin earthquake are shown in Table 5.

As shown in Table 5, under the same amplitude of earthquake, liquid sloshing height and structure displacement of no-isolation and isolation tanks under far-field long-period earthquake action are obviously greater than that under near-field earthquake action, but the differences of wall tensile stress under different kinds of earthquakes is not very obvious. The liquid sloshing height of rubber isolation structure under far-field long-period earthquake is larger, and the reduction effect of sliding isolation on liquid sloshing wave height is better than hybrid isolation. Under far-field long-period earthquake, the possible failure modes of rubber isolation liquid storage tank are excessive displacement and liquid overflow, however, the occurrence probabilities of failure modes of sliding and hybrid isolation liquid storage tanks are low.

5. Conclusions

In order to reduce the probability of earthquake damage of concrete rectangular liquid storage tank, 3-D numerical calculation models of no-isolation, rubber isolation, sliding isolation and hybrid isolation concrete rectangular liquid storage tanks are established, respectively. By comparing dynamic responses of different structures, effectiveness of three kinds of isolation methods is studied. Besides, influences of PGA, bidirectional earthquake and far-field long-period seismic waves on dynamic responses of different structures are investigated. The main conclusions are as follows

- Rubber isolation has a very significant amplification effect on liquid sloshing wave height, but sliding isolation and hybrid isolation can significantly reduce liquid sloshing wave height; the reduction effect of sliding isolation on the wall tensile stress is better than those of rubber isolation and hybrid isolation; and the horizontal displacement of sliding isolation structure with limiting-devices and hybrid isolation structure is much smaller than that of rubber isolation structure.
- Liquid sloshing wave height, wall tensile stress and structure displacement are all increased with the increase of PGA. When PGA is 0.40 g, wall tensile stress of no-isolation structure is close to concrete tensile strength, and liquid sloshing wave height of rubber isolation structure has surpassed the freeboard, which will cause liquid overflow.
- Bidirectional earthquake significantly increases liquid sloshing wave height, wall tension stress and structure displacement. Exceeding probabilities corresponding to liquid sloshing wave height and structure displacement of rubber isolating structure become larger under bidirectional seismic action; liquid sloshing wave height and wall tension stress of sliding isolation with limiting-devices structure and hybrid isolation structure are less affected by the bidirectional earthquake, but structure displacement is still influenced obviously by bidirectional earthquake.
- Influence of far-field long-period seismic wave on the wall tensile stress is small, but its influences on structure displacement and liquid sloshing wave height large, especially for rubber isolation, structure displacement and liquid sloshing wave height are more likely to exceed the limit.
- On the whole, the cost of Teflon sliding isolation structure is the lowest, besides, the control effect of

sliding isolation on concrete liquid storage structure is very significant, so it is a potential damping method for concrete rectangular liquid storage tank.

Acknowledgments

This paper is a part of the National Natural Science Foundation of China (Grant number: 51908267), a part of the China Postdoctoral Science Foundation (Grant number: 2018M633652XB), a part of the Hongliu Outstanding Young Talents Support Program of Lanzhou University of Technology (Grant number: 04-061807), a part of the Open Foundation of International Research Base on Seismic Mitigation and Isolation of Gansu Province (Grant number: GII2019-N03) and a part of the Innovation Ability Improvement Project of Colleges and Universities in Gansu Province (2019A-021).

References

ACI Committee 350 (2006), "Seismic design of liquid-containing concrete structures (ACI 350. 3-01) and commentary (ACI 350. 3R-01)", *American Concrete Institute*, Farmington Hills, U.S.A.

Bagheri, S. and Farajian, M. (2016), "The effects of input earthquake characteristics on the nonlinear dynamic behavior of FPS isolated liquid storage tanks", *J. Vib. Control*, 1-19. https://doi.org/10.1177%2F1077546316655914.

Cancellara, D. and Angelis, F.D. (2016), "Nonlinear dynamic analysis for multi-storey RC structures with hybrid base isolation systems in presence of bi-directional ground motions", *Compos. Struct.*, **154**, 464-492. https://doi.org/10.1016/j.compstruct.2016.07.030.

Chen, Y.H., Hwang, W.S. and Ko, C.H. (2007), "Sloshing behaviours of rectangular and cylindrical liquid tanks subjected to harmonic and seismic excitations", *Earthq. Eng. Struct. Dyn.*, **36**(12), 1701-1717. https://doi.org/10.1002/eqe.713.

Cheng, X.S., Jing, W. and Feng, H. (2019), "Nonlinear dynamic responses of sliding isolation concrete liquid storage tank with limiting-devices", *KSCE J. Civil Eng.*, **23**(7), 3005-3020. https://doi.org/10.1007/s12205-019-1480-5.

Cheng, X.S., Jing, W. and Gong, L.J. (2017), "Simplified model and energy dissipation characteristics of a rectangular liquid-storage structure controlled with sliding base isolation and displacement-limiting devices", *J. Perform. Construct. Facilit., ASCE*, **31**(5), 1-11. https://doi.org/10.1061/(ASCE)CF.1943-5509.0001066.

Cheng, X.S., Jing, W. and Li, X.L. (2018), "Effect of the limiting-device type on the dynamic responses of sliding isolation in a CRLSS", Earthquakes and Structures, **15**(2): 133-144.

Colombo, J.I. and Almazán, J.L. (2017), "Seismic reliability of legged wine storage tanks retrofitted by means of a seismic isolation device", *Eng. Struct.*, **134**(1), 303-316. https://doi.org/10.1016/j.engstruct.2016.12.058.

Compagnoni, M.E., Curadelli, O. and Ambrosini, D. (2018), "Experimental study on the seismic response of liquid storage tanks with sliding concave bearings", *Journal of Loss Prevention in the Process Industries*, **55**: 1-9.

emuru, V.S. M., Nagarajaiah, S., Masroor, A. and Mosqueda, G. (2014), "Dynamic lateral stability of elastomeric seismic isolation bearings", *J. Struct. Eng.*, **140**(8), A4014014. https://doi.org/10.1061/(ASCE)ST.1943-541X.0000955.

Gao, L., Guo, E.D., Wang, X.J., LIU, Z. and HONG, G. (2012), "Earthquake damage analysis of pools in water supply system", *J. Nat. Disasters*, **21**(5),120-126.

Hashemi, S. and Aghashiri M.H. (2017), "Seismic responses of base-isolated flexible rectangular fluid containers under horizontal ground motion", *Soil Dyn. Earthq. Eng.*, **100**, 159-168. https://doi.org/10.1016/j.soildyn.2017.05.010.

Jing, W. and Cheng, X.S. (2019), "Dynamic responses of sliding isolation concrete rectangular liquid storage structure under far-field long-period earthquake", *J. Appl. Flu. Mech.*, **12**(3), 907-919. https://doi.org/10.1007/s13369-017-2814-6.

Li, Z.L., Li, Y. and Li, H.B. (2010), "Parametric research on seismic response of large scale liquid storage tank isolated by lead-rubber bearings", *J. Sichuan Univ.*, **42**(5), 134-141.

Malhotra, P.K. (1997), "New methods for seismic isolation of liquid-storage tanks", *Earthq. Eng. Struct. Dyn.*, **26**, 839-847. https://doi.org/10.1002/(SICI)1096-9845(199708)26:8%3C839::AID-EQE679%3E3.0.CO;2-Y.

Mazza, F. and Mazza, M. (2016), "Nonlinear seismic analysis of irregular r.c. framed buildings base-isolated with friction pendulum system under near-fault excitations", *Soil Dyn. Earthq. Eng.*, **90**: 299-312. https://doi.org/10.1016/j.soildyn.2016.08.028.

Mazza, F., Mazza, M. and Vulcano, A. (2017), "Nonlinear response of r.c. framed buildings retrofitted by different base-isolation systems under horizontal and vertical components of near-fault earthquakes", *Earthq. Struct.*, **12**(1), 135-144. https://doi.org/10.12989/eas.2017.12.1.135.

Moeindarbari, H., Malekzadeh, M. and Taghikhany, T. (2014), "Probabilistic analysis of seismically isolated elevated liquid storage tank using multi-phase friction bearing", *Earthq. Struct*., **6**(1), 111-125. http://dx.doi.org/10.12989/eas.2014.6.1.111.

Mosqueda, G., Whittaker, A.S. and Fenves, G.L. (2004), "Characterization and modeling of friction pendulum bearings subjected to multiple components of excitation", *J. Struct. Eng.*, **130**, 433-442. https://doi.org/10.1061/(ASCE)0733-9445(2004)130:3(433).

Panchal, V.R. and Jangid, R.S. (2011), "Seismic response of liquid storage steel tanks with variable frequency pendulum isolator", *KSCE J. Civil Eng.*, **15**(6), 1041-1055. https://doi.org/10.1007/s12205-011-0945-y.

Rawat, A., Matsagar, V.A. and Nagpal, A.K. (2019), "Numerical study of base-isolated cylindrical liquid storage tanks using coupled acoustic-structural approach", *Soil Dyn. Earthq. Eng.*, **119**, 196-219. https://doi.org/10.1016/j.soildyn.2019.01.005.

Safari, S. and Tarinejad, R. (2016), "Parametric study of stochastic seismic responses of base-isolated liquid storage tanks under near-fault and far-fault ground motions", *J. Vib. Control*, **24**(24), 5747-5764. https://doi.org/10.1177%2F1077546316647576.

Saha, S.K., Sepahvand, K., Matsagar, V.A., Jain, A.K. and Marburg, S. (2013), "Stochastic analysis of base-isolated liquid storage tanks with uncertain isolator parameters under random excitation", *Eng. Struct.*, **57**(4), 465-474. https://doi.org/10.1016/j.engstruct.2013.09.037.

Sezen, H., Livaoglu, R. and Dogangun, A. (2008), "Dynamic analysis and seismic performance evaluation of above-ground liquid-containing tanks", *Eng. Struct.*, **30**(3), 794-803. https://doi.org/10.1016/j.engstruct.2007.05.002.

Shekari, M.R., Hekmatzadeh, A.A. and Amiri, S.M. (2019), "On the nonlinear dynamic analysis of base-isolated three-dimensional rectangular thin-walled steel tanks equipped with vertical baffle", *Thin-Walled Struct.*, **138**, 79-94. https://doi.org/10.1016/j.tws.2019.01.037.

Shrimali, M.K. and Jangid, R.S. (2004), "Seismic analysis of base-isolated liquid storage tanks", *J. Sound Vib*., **275**(1-2), 59-75. https://doi.org/10.1016/S0022-460X(03)00749-1.

Sun, J.G., Hao, J.F., Liu, Y. *et al*. (2016), "Simplified mechanical model for vibration isolation analysis of a vertical storage tank considering swinging effect", *J. Vib. Control*, **35**(11), 20-27.

Sussman. T. and Sundqvist, J. (2003), "Fluid-structure interaction analysis with a subsonic potential-based fluid formulation", *Comput. Struct.*, **81**(8-11), 949-962. https://doi.org/10.1016/S0045-7949(02)00407-8.

Tsipianitis, A. and Tsompanakis, Y. (2019), "Impact of damping modeling on the seismic response of base-isolated liquid storage tanks", *Soil Dyn. Earthq. Eng.*, **121**, 281-292. https://doi.org/10.1016/j.soildyn.2019.03.013.

Uckan, E., Umut, Ö., Sisman, F.N., Karimzadeh, S. and Askan, A. (2018), "Seismic response of base isolated liquid storage tanks to real and simulated near fault pulse type ground motions." *Soil Dyn. Earthq. Eng.*, **112**, 58-68. https://doi.org/10.1016/j.soildyn.2018.04.030.

Yuan, L. (1993), "Finite element analysis of slab rubber bearings for building vibration isolation", *World Rubber Industry*, **21**(6), 1574-1586. https://doi.org/10.21595/jve.2019.20645.

Zama, S. (2004), "Seismic hazard assessment for liquid sloshing of oil storage tanks due to long-period strong ground motions in Japan", *Proceedings of the 13th World Conference on Earthquake Engineering*, Vancouver, B.C., Canada, August 1-6.

Zhang, R.F., Weng, D.G. and Ren, X.S. (2011), "Seismic analysis of a LNG storage tank isolated by a multiple friction pendulum system", *Earthq. Eng. Eng. Vib.*, **10**(2), 253-262. https://doi.org/10.1007/s11803-011-0063-3.

AT